Finite Element Analysis of Viscous Mixing with a Helical Ribbon-Screw Impeller

P. A. Tanguy, R. Lacroix, F. Bertrand, L. Choplin, and E. Brito de la Fuente
Dept. of Chemical Engineering, Laval University, Quebec City, QC, Canada, G1K 7P4

A finite element analysis was carried out to study the mixing patterns of a viscous Newtonian fluid into a stirred tank. A helical ribbon screw impeller (HRS) was used as the mixing device. The numerical simulation involved the full three-dimensional resolution of the equations of change governing the flow in the tank. The circulation time and the torque were determined and compared with experimental data. A good agreement was found, showing the usefulness of the numerical approach for design purposes.

Introduction

Mixing is one of the oldest processing operations used in the chemical industry. This operation is conceptually quite simple and involves an impeller mounted on a motor-driven rotating shaft immersed into a vessel containing the liquid to homogenize. A large number of impellers can be used for the mixing duty, the selection of which depends on the operating conditions such as the agitation speed and the rheological behavior of the fluid.

The design of mixing systems is based mainly on the analysis of integral (or macroscopic) quantities such as circulation time, mixing time, and power consumption, obtained by correlating experimental data (Harnby et al., 1989). The experimental approach is time-consuming and sometimes expensive, and does not provide an efficient pathway to scale-up (design of new equipments) or scale-down (improvement of existing processes).

The study of mixing by numerical methods is quite recent, and the first significant contributions to the field were published in the early 80s (Ottino et al., 1981; Bertrand, 1983). Little progress has been made, because it is quite difficult to develop a universal simulation approach due to the vast variety of mixing devices, all with different behaviors, and the broad range of applications. However, it appears that advances were made recently in the modeling of fermenters. Pericleous and Patel (1987) simulated a stirred biochemical reactor using the finite difference code PHOENICS. The motion of the impeller was represented as sources of angular and/or axial momentum, and various geometrical features of the vessel as sinks. Tragard (1988) developed a turbulent fluid dynamic model to investigate mass transfer into an aerated fermentation reactor provided with a Rushton turbine. Lafon and Bertrand (1988) proposed a two-dimensional finite element model for the prediction of laminar mixing of Newtonian and pseudoplastic fluids with paddles and anchors. More recently, Rubart (1990) also used a finite element approach to determine the power dissipated by blades for various CMC liquids. In those works, the flow was studied in a cross-section of the vessel through two-dimensional simulations. Although these contributions represent a real progress in the field, they do not adequately describe the complex hydrodynamics inherent to industrial mixers, where the flow in general is fully three-dimensional.

The objective of this study is to demonstrate how capable advanced computational fluid dynamics are in dealing with the three-dimensional modeling of flow behavior that causes mixing. The scope of this article is limited to viscous mixing in cylindrical unbaffled vessels: it shows that some mixer design parameters can be computed with reasonable accuracy and the numerical approach provides a very powerful method for the analysis of the mixing flow pattern. The work is based on the finite element resolution of the full three-dimensional equations of change that govern the agitation of a Newtonian fluid in a vessel provided with an helical ribbon screw impeller (HRS) as shown in Figure 1. The speed of rotation will be selected such that the operating conditions are in the laminar mixing region.

Mathematical Model

Equations of change

The equations governing the flow of an incompressible fluid

Correspondence concerning this article should be addressed to P. A. Tanguy.

within a stirred vessel when using an Eulerian viewpoint are the classical Navier-Stokes equations:

$$\rho(\partial v/\partial t + v\cdot\text{grad } v) - \text{div } \pi = f, \tag{1}$$

$$\text{div } v = 0, \tag{2}$$

$$\pi = -p\delta + \tau. \tag{3}$$

where v is the velocity, p the pressure, f a body force, δ the unit tensor, and ρ the density; τ is a function of the velocity field expressed by a rheological equation of state. In this work, we consider the simple Newton's law of viscosity:

$$\tau = -2\mu\dot{\gamma}, \tag{4}$$

$$\dot{\gamma} = 1/2[\nabla v + (\nabla v)^T], \tag{5}$$

where μ is the Newtonian viscosity. These equations must be completed with appropriate boundary conditions for mathematical closure.

Discretization

The discretization is carried out using the finite element method. This requires the selection of interpolation functions for the velocity and the pressure. In a fluid flow context, not any approximation of velocity can be mixed with any approximation of pressure. The theoretical compatibility condition for mixed methods, called the Brezzi condition (Brezzi, 1974), must be satisfied to ensure reliable computations. If this condition were not satisfied, the velocity results in general are still acceptable, but the pressure results may suffer from spurious modes that can sometimes be filtered out (Sani et al., 1981; Fortin and Boivin, 1987). An element shape must also be chosen. Hexahedral elements or bricks are a natural choice for structured meshes, while unstructured grids are best described with tetrahedra.

When meshing a very complex flow domain such as a vessel provided with an HRS impeller, the use of hexahedra is quite impracticable because of the presence of extremely distorted elements in the vicinity of the impeller. In the present study, the tetrahedral element $P_1^+ - P_0$ (Figure 2) is used. This element, which was introduced recently for the computation of incompressible fluid flow (Bertrand et al., 1992), is based on the classical linear tetrahedron $P_1 - P_0$ (linear velocity, constant pressure), on which additional degrees of freedom are added at the middle of each face enabling the control of mass within the element. This tetrahedral counterpart of the $Q_1^+ - P_0$ hexahedron (Robichaud et al., 1987) satisfies the Brezzi compatibility condition at the element level, ensuring that correct velocities and pressure can be computed.

Boundary conditions

When using the Eulerian viewpoint, it is very difficult to impose the boundary conditions due to the presence of a moving boundary in a fixed mesh. This problem is unsteady in nature, although periodic, and thus requires either a remeshing or at least a moving of the mesh at each time step, which is very costly.

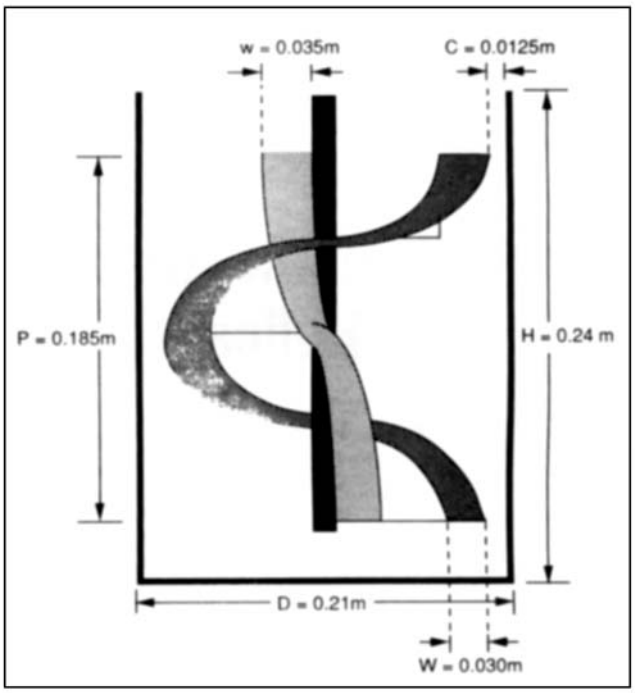

Figure 1. Helical ribbon screw impeller.

In a cylindrical vessel without baffles such as the one that is considered here, the symmetry of revolution of the domain incites us to choose an alternate viewpoint that drastically simplifies the imposition of the boundary conditions, that is the one of an observer moving with the impeller (Figure 3). This is a Lagrangian viewpoint in a non-Galilean frame of reference, (the observer is in rotation) where not only do the boundary conditions have to be modified, but so does the set of equations of change. Indeed, the resulting flow belongs to the class of geostrophic flows. Consequently, the centrifugal and the Coriolis forces now appear in the standard Navier-Stokes equations (Tritton, 1988). Two dimensionless numbers can be used to evaluate the degree of importance of these two forces in the context of mixing: the Eckman number, $\mu/\Omega L^2$; the Rossby number, $U/\Omega L$, where Ω is the rotation speed, and U and L a characteristic velocity and a characteristic length, respectively. In the present work, both Eckman and Rossby numbers are of the order of unity, meaning that the Coriolis and the centrifugal forces cannot be neglected.

If in the Eulerian viewpoint, the flow were assumed fully periodic and there were no flow bifurcations, then in the new frame of reference, the fluid flow can be treated at steady state. Consequently, the new form of the momentum equation (Eq. 1) is:

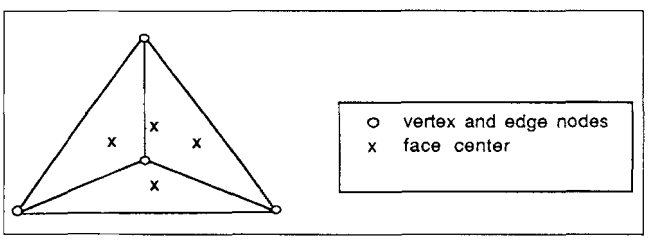

Figure 2. Enriched tetrahedral element.

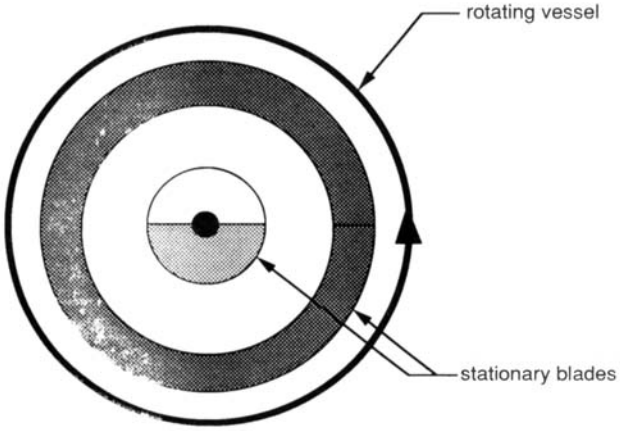

Figure 3. Non-Galilean Lagrangian frame of reference (top view of the vessel).

$$\rho[v\cdot\text{grad } v+\omega\times(\omega\times r)+2\omega\times v]-\text{div } \pi=f, \qquad (6)$$

where ω is the angular velocity, r the radius, $\omega\times(\omega\times r)$ the centrifugal force, and $2\omega\times v$ the Coriolis force.

Due to the fully three-dimensional nature of the flow and the lack of a symmetry plane, the computational domain consists of the whole vessel. Cartesian coordinates in three dimensions are used to express the differential operators in the governing equations. Boundary conditions for the velocity are quite simple and consist of Dirichlet conditions (rotational speed) on the walls, homogeneous Dirichlet conditions (stick condition) on the impeller and the shaft, and zero normal velocity at the fluid surface. The thickness of the impeller blade is assumed to be negligible.

Solid model and finite element mesh

A major difficulty in the three-dimensional numerical modeling of the flow in mixing devices is the generation of the mesh. In the present work, the generation of the solid model (geometry) and the mesh were performed using PATRAN PLUS software from PDA Engineering. The fluid domain was meshed in two steps. The first step consisted of generating the mesh around the impeller in a chunkwise fashion, each chunk corresponding to a part of the domain (hyperpatch in PATRAN terminology); 156 hyperpatches were necessary to describe accurately this volume. The second step consisted of meshing the volume located below the impeller, that is, between the shaft tip and the vessel bottom. Five additional hyperpatches were created in that region. Great care was taken to get element and nodal compatibility between steps 1 and 2.

As PATRAN PLUS software cannot generate automatically $P_1^+ - P_0$ elements, linear elements were generated first, and the extra degrees of freedom were added at the middle of each face through a customized program. The final mesh included 12,928 elements yielding 81,303 velocity and 12,928 pressure degrees of freedom. Figure 4 shows a wire-frame representation of the surface mesh.

Numerical algorithm

Let us first consider the steady Stokes flow as described by the following equations:

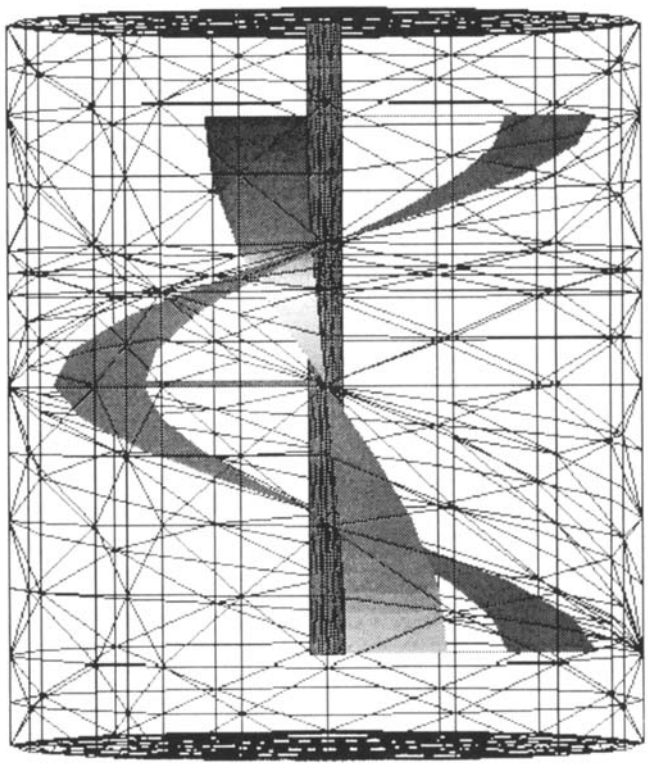

Figure 4. Finite element mesh (surface representation).

$$\text{div } \pi=f, \qquad (7)$$

$$\text{div } v=0. \qquad (8)$$

It can be shown that the resolution of this system is equivalent to that of a saddle-point problem (Fortin and Glowinski, 1983):

$$\underset{v\in V}{\text{Min}}\ \underset{p\in Q}{\text{Max}}\frac{1}{2}\int_\Omega \mu|\dot\gamma(v)|^2 d\Omega-\int_\Omega p\ \text{div } v\ d\Omega-\int_\Omega fv\ d\Omega, \qquad (9)$$

which leads to the following weak formulation:

$$a(v,\psi)-b(\psi,p)=(f,\psi), \quad \forall\psi\in V, \qquad (10)$$

$$b(v,\phi)=0, \quad \forall\phi\in Q, \qquad (11)$$

where V and Q are the velocity and pressure vector spaces, respectively, and where

$$a(v,\psi)=\int_\Omega \mu\dot\gamma(v)\dot\gamma(\psi)\ d\Omega, \qquad (12)$$

$$b(v,\phi)=\int_\Omega \phi\ \text{div } v\ d\Omega, \qquad (13)$$

$$(f,\psi)=\int_\Omega f\psi\ d\Omega. \qquad (14)$$

From a practical viewpoint, the solution of problem (Eqs. 10–11) leads to the following matrix problem:

$$Av - B^T p = F, \tag{15}$$

$$Bv = 0, \tag{16}$$

where v and p denote the velocity and the pressure vectors, respectively, A the viscous matrix, and B the divergence operator.

The above matrix problem can now be extended by incorporating the extra terms corresponding to convection, centrifugal and Coriolis forces, which yield:

$$Av - B^T p = F - C(v)v, \tag{17}$$

$$Bv = 0. \tag{18}$$

In Eq. 17, A includes the contribution of the Coriolis force and F the contribution of the centrifugal force. The trilinear form $C(v)v$ is nothing but the matrix representation of the advection.

The resolution of the matrix system is carried out using an iterative solver, the Incomplete Uzawa algorithm (Robichaud et al., 1990). The first step of the method consists of solving Eq. 17 by a preconditioned gradient method, P being given. The resulting velocity field is then projected onto a divergence-free subspace, and the pressure is updated at that level. The advantage of the incomplete Uzawa algorithm over a direct method is twofold. First, the storage requirement is much smaller due to the use of an incomplete factorization (about 8 megabytes per 10,000 equations) enabling the use of engineering workstations as computational platforms. Secondly, the CPU time to get the solution varies as $NEQ^{1.3}$ with the proposed method, as compared to $NEQ^{2.33}$ with a direct solver, where NEQ stands for the number of equations.

Case Study

The geometrical characteristics of the impeller and the vessel (Figure 3) are shown in Figure 1. The fluid is a solution of glycerol (95%) and water (5%), and its viscosity is 0.55 Pa·s at θ = 12°C. The tests are performed at 10, 20, 30 and 40 rpm, with the impeller moving in the clockwise direction. At these velocities, the upper surface of the fluid in the vessel is horizontal.

Results

The following experimental and numerical results are compared on the basis of circulation time and torque.

From an experimental viewpoint, circulation time t_c can be estimated using a thermal technique (Hoogendoorn and Den-Hartog, 1967; Brito de la Fuente, 1992). First, a small amount of the same, but heated, fluid (2% of the total fluid volume in the agitated vessel) is injected in the tank just below the surface in the vicinity of the shaft. The evolution of the fluid temperature is then scanned by using thermistor probes. In our experiments, the temperature of the injected fluid was kept constant (60°C), and the small effect on viscosity due to a global increase of temperature from around 11°C to 12.5°C was considered as negligible. In addition, buoyant effects due to the presence of a small amount of heated fluid were neglected. From the response curves, three characteristic times

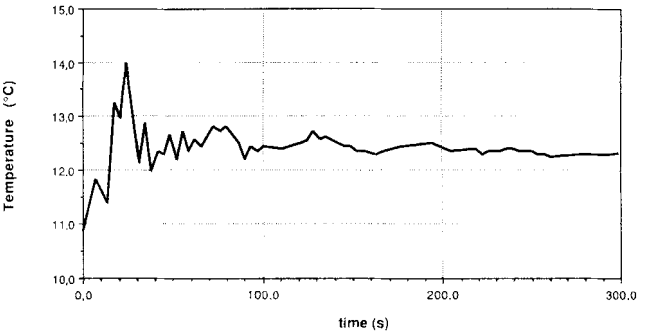

Figure 5. Typical experimental thermogram (N = 20 rpm).

can be estimated: the mixing time t_M (time for the curve to smooth out); the circulation time t_c (time between two consecutive peaks); and a lag time t_l (elapsed time between the injection time and the first peak). Only t_c will be compared here with the numerical results, since it is easier to evaluate on the thermogram (Figure 5). Finally, the torque is directly measured on the shaft by a torquemeter.

From a numerical standpoint, it is possible to mimic the thermal method as follows: the trajectory of neutrally buoyant particles from a given origin (in practice, the same location as the above injection point) can be computed by integrating over time the velocity with a variable-step second-order Runge-Kutta method. An "equivalent" thermogram can be obtained, which consists of plotting the time evolution of the distance between the particle and a given fixed reference point located at the position of the experimental thermal probe. The "signal," distance vs. time, thus obtained (Figure 6) exhibits peaks similar to those of a real thermogram.

Furthermore, the torque can be obtained by computing:

$$T = -\int_S [(n \cdot \pi) \times r \, ds] \tag{19}$$

where S is the surface of the vessel, and n the normal to the surface.

Table 1 summarizes both the experimental and numerical results. It can be observed that the agreement for the circulation time is quite good, and even more so considering the relative accuracy of the numerical simulation and the uncertainty (about 5 s) on the experimental circulation time. A classical result

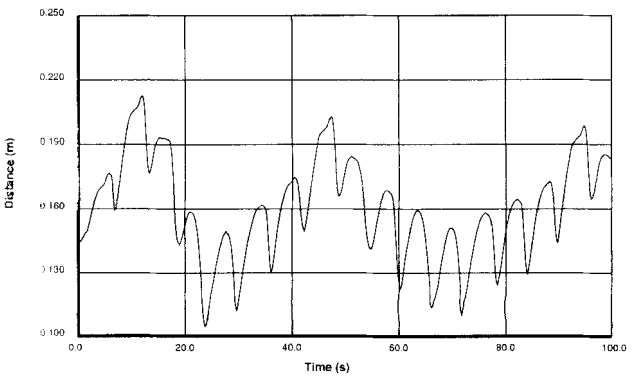

Figure 6. Tracer signal at 20 rpm.

Table 1. Variation of Circulation Time and Torque with the Rotation Speed

Impeller Velocity (RPM)	Numerical Circulation Time (s)	Experimental Circulation Time (s)	Numerical Torque (N·m)	Experimental Torque (N·m)
10	110	104	0.013	0.014
20	48	51	0.026	0.040
30	29	35	0.041	0.068
40	22	25	0.056	0.095

indicates that the circulation time should be proportional to the rotation speed in the laminar regime (Ulbrecht and Carreau, 1985), as shown in Figure 7.

The comparison of the torque results shows that the predicted values are within the same order of magnitude as the experimental ones. Better accuracy of the numerical simulation could be obtained by the use of a finer mesh, especially at the largest value of the Reynolds number.

The circulation pattern obtained at 10 rpm is shown in Figure 8. The arrows indicate the direction of circulation along the calculated trajectory. First, the trajectory of the "fluid particle" follows a tangential pattern combined with a radially inward component; then the fluid particle is pumped down to the bottom and is submitted to another tangential and radially outward action, before being pumped back up to the top in a spiral-like motion at the periphery of the reservoir by the action of the ribbon. This completes a circulation loop. In terms of flow pattern, its primary component is helical due essentially to the ribbon. A secondary component is created mainly by the combined action of the shape of the impeller (the axial pumping is upward at the periphery and downward at the center of the reservoir) and the centrifugal forces generated by the primary tangential flow.

One manifestation of mixing is that closed circulation loops should not be present (quasi-periodic flow). As a consequence, the concept of circulation time should be understood as a mean circulation time with some scattering reflecting the complexity of the flow pattern within the tank. To characterize this scattering, a numerical experiment was carried out that consisted of calculating the loop time at various injection points with the intent of assessing the homogeneity of the spatial distribution of circulation times within the vessel. The circulation time computed at six different locations (two at the top, two at mid-height, and two at the bottom) gave the following results: at 10 rpm, $105 < t_c < 160$ s; at 20 rpm, $51 < t_c < 76$ s; and at 30 rpm, $35 < t_c < 41$ s. At 40 rpm, the presence of two separated mixing zones with nearly no exchange between them (Figure 9) made it impossible to determine an average circulation time.

It now becomes clear that the science of mixing may benefit a lot from numerical simulations. Indeed, its use in conjunction with experimental work allows a thorough analysis of the flow pattern in such a way that it enables us to assess preferential mixing zones, dead zones, caverns, and so on.

As a good illustration, an interesting phenomenon was observed about the impact of the screw on the fluid motion at the bottom of the vessel. The presence of an inner screw is supposed to enhance the axial pumping effect on the fluid from the top to the bottom in the present case, since the impeller rotates in the clockwise direction (the screw pushes down the

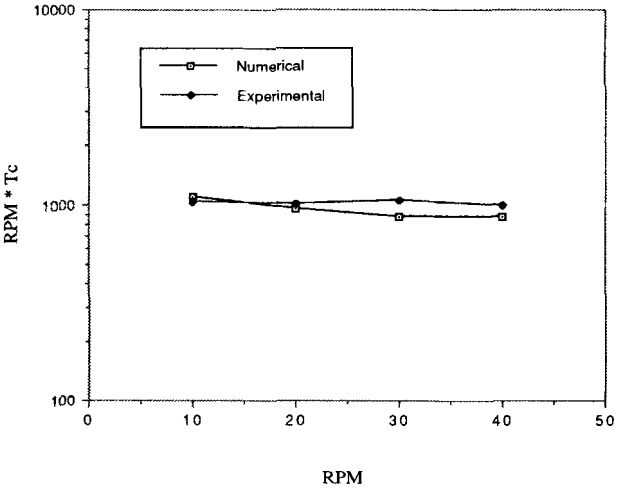

Figure 7. Variation of the circulation time with the rotation speed.

fluid). It could also be thought that this enhancement increases with the rotation speed. The reverse effect was noticed. At a low speed (10 rpm), the screw fully played its purpose. At 20 rpm, a stagnant zone developed at the bottom and its size increased with an increasing speed. At 40 rpm, the fluid motion became opposite to the screw at the vicinity of the shaft tip (Figure 10)!

Finally, let us mention that the simulations were performed on a 4D/240 Powerserver from Silicon Graphics. The total storage was about 64 megabytes and the execution time about 1 hour per run.

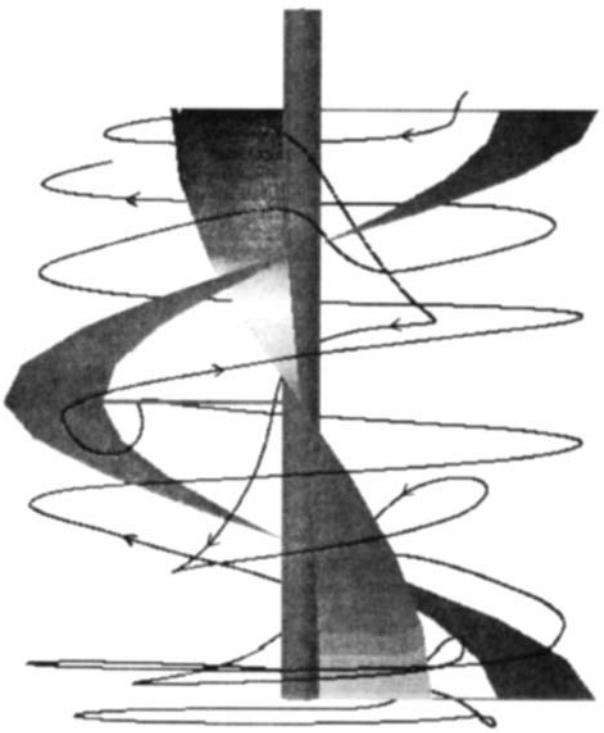

Figure 8. Flow pattern at 10 rpm.

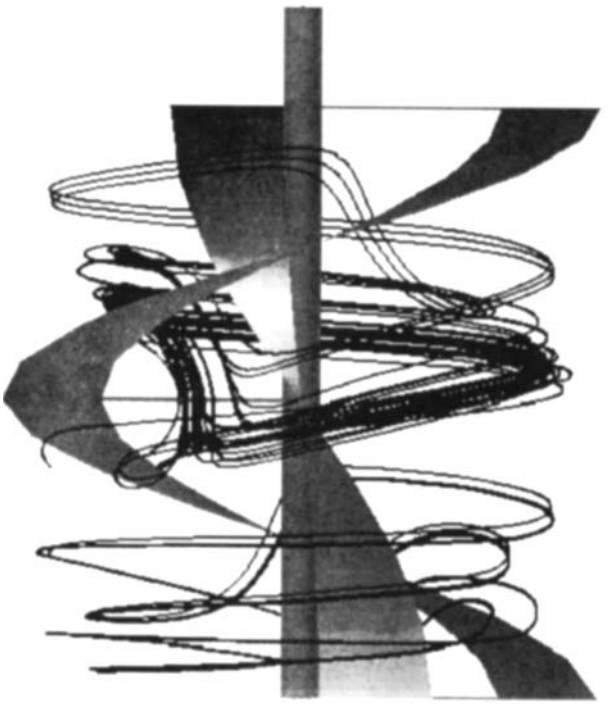

Figure 9. Flow pattern at 40 rpm.

Figure 10. Flow anomaly at the vessel bottom at 40 rpm.

Conclusion

A full three-dimensional resolution of the flow equations provides an efficient way to tackle mixing problems at low cost. In particular, the circulation time, the torque, and flow patterns were easily computed, and the comparison with experimental data exhibited a fairly good agreement. Consequently, we believe that this approach paves the way to modeling more complex mixing systems with non-Newtonian fluids, which are typical of the chemical process industry.

Literature Cited

Bertrand, F., M. Gadbois, and P. A. Tanguy, "Tetrahedral Elements for Fluid Flow," *Int. J. Num. Meth. Eng.*, **33**, 1521 (1992).

Bertrand, J., "Agitation de Fluides Visqueux: Cas de Mobiles à Pales, d'Ancres et de Barrières," Doctoral Thesis, INP Toulouse (1983).

Brezzi, F., "On the Existence, Uniqueness and Approximation of Saddle-Point Problems Arising from Lagrangian Multipliers," *RAIRO, Série Analyse Numerique*, **8**, 129 (1974).

Brito de la Fuente, E., PhD Thesis, Laval University, Quebec, in preparation (1992).

Fortin, M., and R. Glowinski, *The Augmented Lagrangian Method*, North-Holland, Amsterdam (1983).

Fortin, M., and S. Boivin, "A Stabilization Method for Some Finite Element Approximations of Incompressible Flows," *Numerical Methods in Laminar and Turbulent Flow*, C. Taylor, W. G. Habashi, and M. M. Hafez, eds., Vol. 5, Part II, p. 81, Pineridge Press (1987).

Harnby, N., M. F. Edwards, and A. W. Nienow, *Mixing in the Process Industries*, Butterworths (1989).

Hoogendoorn, C. J., and A. P. Den-Hartog, "Model Studies in the Viscous Flow Region," *Chem. Eng. Sci.*, **22**, 1689 (1967).

Lafon, P., and J. Bertrand, "A Numerical Model for the Prediction of Laminar Mixing," *Proc. Eur. Conf. on Mixing*, BHRA, p. 493 (1988).

Ottino, J. M., W. E. Ranz, and C. W. Macosko, "A Framework for Description of Mechanical Mixing of Fluids," *AIChE J.*, **27**, 565 (1981).

Pericleous, K. A., and M. K. Patel, "The Modelling of Tangential and Axial Agitators in Chemical Reactors," *PhysicoChem. Hydrodyn.*, **8**, 105 (1987).

Robichaud, M. P., and P. A. Tanguy, "Comparison of Three-Dimensional Finite Elements for Fluid Flow," *Comm. Appl. Num. Math.*, **3**, 223 (1987).

Robichaud, M. P., P. A. Tanguy, and M. Fortin, "An Iterative Implementation of the Uzawa Algorithm for 3D Fluid Flow Problems," *Int. J. Num. Math. Fluids*, **10**, 429 (1990).

Rubart, L., "Finite Element Analysis of Shear-Thinning Flow Problems in Mixing Vessels," *Proc. Eur. Rheology Conf.*, p. 413, D. R. Oliver, ed., Elsevier (1990).

Sani, R., P. Gresho, R. Lee, D. Griffiths, and M. Engelman, "The Cause and Cure (?) of the Spurious Pressures Generated by Certain FEM Solutions of the Incompressible Navier-Stokes Equations: 1 and 2," *Int. J. Num. Math. Fluids*, **1**, 17 and 171 (1981).

Tragard, Ch., "A Hydrodynamic Model for the Simulation of an Aerated Agitated Fed-Batch Fermentor," *Proc. Int. Conf. on Bioreactor Fluid Dynamics*, p. 117, R. King, ed., Elsevier (1988).

Tritton, D. J., *Physical Fluid Dynamics*, Oxford (1988).

Ulbrecht, J. J., and P. J. Carreau, "Mixing of Viscous Non-Newtonian Liquids," *Mixing of Liquids by Mechanical Agitation*, Vol. 1, Chap. 4, J. J. Ulbrecht and G. K. Patterson, eds., Gordon and Breach Science Publishers (1985).

Manuscript received Jan. 7, 1992, and revision received Apr. 14, 1992.